Scientia Iranica C (2021) 28(3), 1400–1413

Sharif University of Technology
Scientia Iranica
Transactions C: Chemistry and Chemical Engineering
http://scientiairanica.sharif.edu

Sulfated polysaccharide coated $BaFe_{12}O_{19}$: A magnetically separable bifunctional catalyst for the synthesis of benzopyranopyrimidines derivatives and its antibacterial activity evaluation

S. Amirnejat and S. Javanshir[*]

Heterocyclic Chemistry Research Laboratory, Department of Chemistry, Iran University of Science and Technology, Tehran, P.O. Box 1684613114, Iran.

Received 3 March 2020; received in revised form 18 August 2020; accepted 7 December 2020

KEYWORDS
Marine sulfated polysaccharide;
Barium hexaferrite;
Magnetic nanoparticle;
Benzopyranopyrimidines;
Heterogeneous catalyst;
Green chemistry.

Abstract. Marine sulfated polysaccharide Irish Moss (IM) coated $BaFe_{12}O_{19}$ nanocomposites were synthesized and characterized by a Fourier Transform Infrared Spectrometer (FT-IR), Scanning Electron Microscope (SEM), X-Ray Diffraction (XRD), Vibrating-Sample Magnetometer (VSM), and Thermal Gravimetric Analysis (TGA). The indisputable privilege of $BaFe_{12}O_{19}$@IM as a recyclable acid-based bifunctional catalyst has been studied in the preparation of benzopyranopyrimidines via a pseudo-four-component reaction of salicylic aldehydes, malononitrile, and various amines. A catalytic amount of $BaFe_{12}O_{19}$@IM has shown high catalytic activity and stability with negligible detriment in its efficiency over five catalytic cycles. The catalytic property-catalytic performance associations clearly showed the synergistic effect between Irish moss, as the major active phase, and barium ferrite nanoparticles, enabling catalyst separation in a magnetic field. Along with the catalytic activity, a study on the antibacterial performance of $BaFe_{12}O_{19}$@IM nanocomposites on bacteria strains was evaluated. The results showed that the prepared nanocomposites possess antibacterial activity against Gram-positive *Staphylococcus aureus* (*S. aureus*).

1. Introduction

Today, magnetic nanoparticles (MNPs) are noteworthy in the development of various heterogeneous nano catalytic systems with increased biocompatibility [1–4]. Among various magnetic materials reported in the literature, barium hexaferrites are the most widely used permanent magnets and still promising because of their chemical and thermal stability, low production cost, and corrosion resistivity, besides their nontoxicity [5–10]. However, bare magnetic particles tend to be readily aggregated which can be avoided by using different organic or inorganic coatings on the core/shell frame or by using synthetic polymers or natural polysaccharides as capping agents [11–19]. Natural polysaccharides IM or carrageenan moss extracted from red algae comprise nearly one sulfate monoester group per sugar unit. The

---

[*] *Corresponding author. Tel.: +98 21 77240346; Fax: +98 21 73227707*
E-mail addresses: sara_amirnejat@yahoo.com (S. Amirnejat); shjavan@iust.ac.ir (S. Javanshir)

doi: 10.24200/sci.2020.55606.4312

acidic characteristic of carrageenan, which is caused by its high sulfate content, accounts for many of its important properties [20–22]. It is important to mention that they are strongly anionic polymers because of their half-ester sulfate segments (Figure 1) [23]. Both sulfate and hydroxyl groups as Brønsted-Lowry basic and acidic sites render IM an effective catalytic for organic reactions. In addition, polymer-inorganic nanocomposites due to their biodegradability, non-toxicity, thermal and chemical stability constitute a new platform for the design of heterogeneous catalysts [24–28].

Due to the various applications of benzopyranopyrimidine scaffolds, such as cytotoxic activity against cancer cell lines [29], anti-aggregating, anti-fungal, antimicrobial activities [30,31], and their fundamental pharmacological properties, special attention has been paid to the synthesis of benzopyranopyrimidine scaffolds as an impressive class of heterocycles [32–42].

In continuation of this research, the catalytic activity of hybrid nanocomposites based on natural polysaccharides IM in several multicomponent reactions (MCRs) has been investigated [18,19]. In the present work, $BaFe_{12}O_{19}$@IM as a novel and reusable biomagnetic heterogeneous nanocatalyst was prepared and used in the synthesis of benzopyranopyrimidine derivatives through one-pot multicomponent condensation of salicylaldehyde derivatives **1a–g**, malononitrile (**2**), and secondary amine **3a–e** at ambient temperature (Figure 2). The present study demonstrates that the prepared nano biocatalyst have high thermal and chemical stability, ferromagnetic property, and easy renewability. On the other hand, in recent decades, antibacterial compounds containing metallic nanoparticles have been the subject of growing research to counter the resistance of microorganisms to antibiotics. Therefore, the antibacterial activity of the designed nanocomposites against two bacterial strains was investigated.

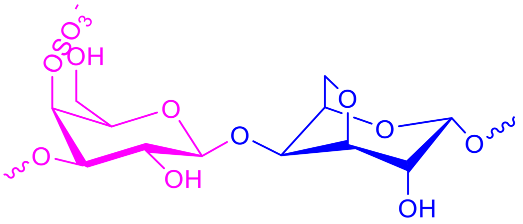

Figure 1. Chemical structure of carrageenan moss.

2. Experimental

2.1. *Materials and methods*

All materials were purchased from Merck or Sigma Aldrich and used without further purification. IR spectra were recorded using KBr discs on a Shimadzu FT-IR-470 spectrophotometer. X-Ray Diffraction (XRD) measurements were carried out using a Philips analyzer, and the calcination of the catalyst was performed using an Exciton oven. Magnetic measurements were performed using VSM model MDKFD from Danesh Pajohan Kavir Co., Kashan. The FESEM images were recorded using a ZEISS instrument, SIGMA VP model, Germany. The ^1H and ^{13}C spectra were recorded on a Bruker DRX 500-Avance (500 and 125 MHz, respectively) in $CDCl_3$, internal standard-TMS. Melting points were determined by electro thermal 9100 apparatus and are uncorrected. Sonication for synthesis of the catalyst was performed by Elma at 60 Hz. Thermogravimetric analyses (TGA) were performed by the D-32609 Hullhorst apparatus.

2.2. *Synthesis of barium hexaferrite magnetic nanoparticles*

Barium hexaferrite magnetic nanoparticles ($BaFe_{12}O_{19}$) were prepared using a sol-gel method. For this purpose, an aqueous solution of barium ferrite was prepared by dissolving barium nitrate ($Ba(NO_3)_2$ (0.52 g, 1.99 mmol), and ferric nitrate.nonahydrate ($Fe(NO_3)_3.9H_2O$) (9.6 g, 23.76 mmol) in 100 ml of deionized water, followed by the addition of citric acid (4.5 g) under vigorous stirring. In order to achieve a stable dispersion, the mixture was sonicated for 15 min using an ultrasonic bath. The pH of the solution was then adjusted to 8.0 by adding an ammonia solution (25%), and the mixture was oven dried at 80°C. The

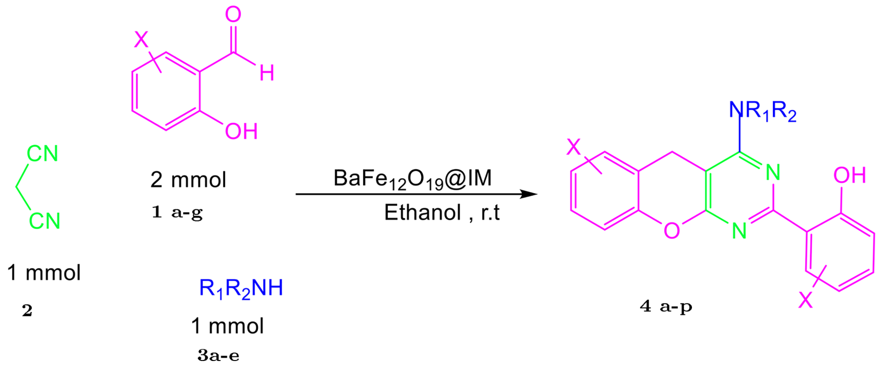

Figure 2. Synthesis of benzopyranopyrimidines in the presence of $BaFe_{12}O_{19}$@IM magnetic nanocatalyst.

product was calcinated at 750°C for 2 h to furnish the desired $BaFe_{12}O_{19}$ magnetic nanoparticles.

2.3. *Preparation of $BaFe_{12}O_{19}$@IM nanocomposite*

Irish moss (7.8 g) and synthetic $BaFe_{12}O_{19}$ (3.12 g, 2.8 mmol) were added to a mixture of H_2O: ETOH (15 ml, 2:1). The mixture was stirred for 2 h and thereafter sonicated for 40 min. After evaporation of the solvent, the obtained $BaFe_{12}O_{19}$/IM was oven dried for 6h nanocomposite (Figure 3).

2.4. *General procedure for synthesis of benzopyranopyrimidine derivatives*

A mixture of salcilaldehyde (2 mmol), malononitrile (1 mmol), secondary amines (1 mmol) and $BaFe_{12}O_{19}$@IM nanocomposites (15 mg) in EtOH (4 ml) was stirred at room temperature for 1 h. The reaction advancement was monitored by TLC (eluent, EtOAc/n-hexane, 1:3). At the end of the reaction, the catalyst was collected by an external magnet, and washed for the next experiment. The precipitate was washed several times with DI water and EtOH to obtain the pure product.

2.5. *Spectral data of the selected products*

2-(4-morpholino-5H-chromeno[2,3-d]pyrimidin-2yl)phenol(4a)

Yellow solid; mp. 197-199°C: IR (KBr): 3300, 2856, 2949, 1610, 1535, 1440, 1384, 1388, 1251, 1118, 1110, 1018, 946, 864, 823, 754 cm^{-1}. ^{1}HNMR (500 MHz, $CDCl_3$) ppm: 3.48–3.50 (t, J = 4.9 Hz, 4H), 3.90–3.92 (t, J = 4.8 Hz, 4H), 3.91 (s, 2H), 6.90–6.93 (t, J = 7.4 Hz, 1H), 6.97–6.98 (d, J = 8.15 Hz, 1H), 7.10–7.13 (t, J = 7.1 Hz, 1H), 7.17–7.21 (t, J = 8.3 Hz, 2H), 7.24–7.27 (m, 1H), 7.34–7.37 (t, J = 8.1 Hz, 1H), 8.38–8.40 (d, J = 7.8 Hz, 1H), 13.11 (s, 1H) ; ^{13}CNMR (125 MHz, $CDCl_3$)^{TM} ppm: 25.7, 48.8, 66.8, 76.9, 77.1, 77.4, 97.8, 117.2, 117.7, 119.0, 119.2, 124.6, 128.5, 128.6, 129.3, 133.1, 150.6, 160.5, 162.3. m/z: 361.14 (M+). Anal. Calcd for $C_{21}H_{19}N_3O_3$: C, 69.79; H, 5.30; N, 11.63; O, 13.28.

4-chloro-2-(7-chloro-4-morpholino-5H-chromeno[2,3-d] pyrimidin-2-yl)phenol (4h)

Yellow solid; mp. 249-251°C: IR (KBr): 3735, 3305, 3041, 1649, 1548, 1469, 1240, 1135, 1018, 939, 860, 819, 730, 669 cm^{-1}: ^{1}HNMR (500 MHz, $CDCl_3$) ppm: 3.47 (t, J = 5.0 Hz, 4H), 3.84 (t, J = 5.0 Hz, 4H), 3.90 (s, 4H), 6.85–6.87 (d, J = 8.7 Hz, 1H), 7.07–7.09 (d, J = 8.6 Hz, 1H), 7.17 (s, 1H), 7.19–7.21 (d, J = 8.7 Hz, 1H), 7.23–7.25 (d-d, J = 2.6 Hz, 1H), 8.26 (s, 1H), 12.97 (s, 1H); ^{13}CNMR (125 MHz, $CDCl_3$) ppm: 25.4, 48.6, 64.0, 66.6, 97.7, 118.4, 118.6, 119.1, 119.3, 120.5, 123.8, 128.1, 128.5, 128.9, 129.6, 132.8, 148.7, 158.9, 161.0,164.8. m/z: 429.06 (M+). Anal. Calcd for $C_{21}H_{17}Cl_2N_3O_3$: C, 58.62; H, 3.98; Cl, 16.48; N, 9.77; O, 11.15.

5-methoxy-2-(8-methoxy-4-morpholino-5H-chromeno[2,3-d] pyrimidin-2-yl)phenol (4o)

White solid; mp. 210-213°C: IR (KBr): 3500, 2900,

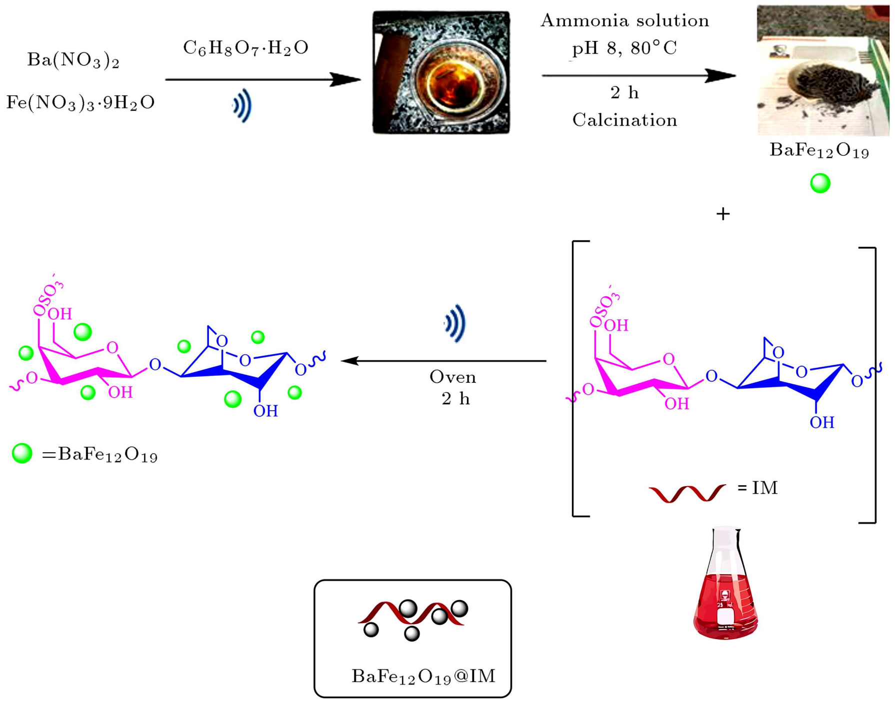

Figure 3. Preparation of $BaFe_{12}$ O_{19}@IM nanocomposite.

2846, 1590,1522, 1435, 1368, 1276, 1204, 1108,1023 , 813, 617 cm^{-1}; ^{1}HNMR (500 MHz, $CDCl_3$) ppm: 3.44 (m, 4H), 3.79 (s, 6H), 3.83 (s, 2H),3.88 (t, $J = 4.4$ Hz, 4H), 6.45–6.48 (m, 2H), 6.66 (d-d, $J = 2.35$ Hz, 1H), 6.70 (s, 1H), 7.05 (d, $J = 8.4$ Hz, 1H), 8.26 (d, $J = 8.75$ Hz, 1H), 13.29 (s, 1H); ^{13}CNMR (125 MHz, $CDCl_3$) ppm: 24.8, 48.6, 55.3, 55.4, 66.6, 97.1, 101.2, 102.0, 106.6, 110.9, 111.1, 111.7, 129.0, 130.4, 151.0, 159.6, 161.9, 162.1, 163.6, 164.7. m/z: 421.16 (M+). Anal. Calcd for $C_{23}H_{23}N_3O_5$: C, 65.55; H, 5.50; N, 9.97; O, 18.98.

3. Results and discussion

The biomagnetic $BaFe_{12}O_{19}$@IM was synthesized according to the method described in Figure 3 Referring to the synthesis strategy presented, barium ferrite nanoparticles were first synthesized, and then the IM was added to the reaction mixture and sonicated for 40 min. The resulting precipitate was then dried to obtain $BaFe_{12}O_{19}$@IM magnetic nanocomposites. The synthesized $BaFe_{12}O_{19}$@IM was characterized using FT-IR spectroscopy, TGA analysis, VSM analysis, SEM image, and XRD analysis.

3.1. Characterization of the nanocomposites

3.1.1. FT-IR analysis

FTIR spectra of $BaFe_{12}O_{19}$ nanoparticles, IM, and $BaFe_{12}O_{19}$@IM nanocomposites were exposed in Figure 4. The peaks at 426.1 and 584.0 cm^{-1} in the IR spectrum of $BaFe_{12}O_{19}$ are related to the metal-oxide stretching vibration originated from the $BaFe_{12}O_{19}$ crystalline structure. The broad absorption band at 3400 cm^{-1} corresponds to the stretching vibrations of the O-H groups, and the absorbance peaks at 1650.7 and 1537.6 cm^{-1} are due to the bending vibrations of hydroxyl groups. In the IM spectrum, absorption bands at $\sim$ 1249 cm^{-1} are attributed to S-O asymmetric stretching in the sulphate group, absorption bands at $\sim$ 1010 and 1065 cm^{-1} are credited to C-O and C-OH stretching and 842.4 cm^{-1}, α(1,3) D-galactose C-O-S stretching vibrations. By conferring on the $BaFe_{12}O_{19}$ @IM spectrum, the presence of the metal oxide absorption bands at 426.1 and 584.0 cm^{-1} and all the absorption bands coherent with IM confirms that the chemical structure of the polysaccharide and of the nanoparticles of $BaFe_{12}O_{19}$ has been preserved after the heat treatments. Furthermore, it is clearly shown that its structure is preserved after recycling.

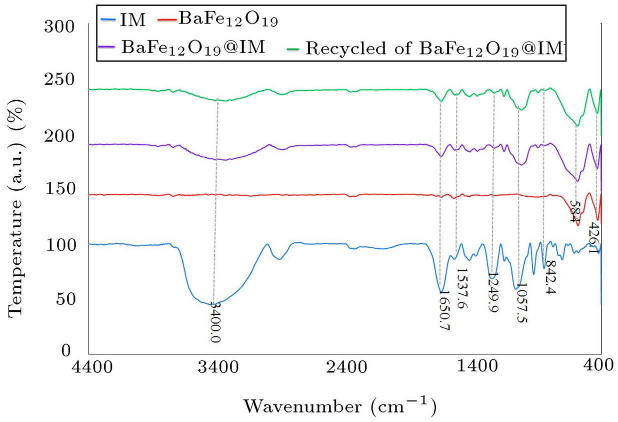

Figure 4. FTIR analysis of the $BaFe_{12}O_{19}$ nanoparticles, IM, and $BaFe_{12}O_{19}$@IM nanocomposite.

3.1.2. Thermogravimetric analysis (TGA)

The TGA analysis for IM, $BaFe_{12}O_{19}$ and $BaFe_{12}O_{19}$@IM was performed to investigate their thermal stability (Figure 5). The samples were heated from ambient temperature to 600°C at a constant heating rate. As can be seen in the IM TGA curve, there is a two-step decomposition for IM. The first weight loss up to $\sim$ 200°C is attributed to loss of adsorbed water. The subsequent weight loss occurring between 200 and 600°C, at about $\sim$ 25%, can be attributed to the degradation of the polysaccharide. In comparison with IM, $BaFe_{12}O_{19}$@IM nanoparticles showed an appropriate resistance to the decomposition up to 300°C. This resistance is due to the existence of $BaFe_{12}O_{19}$ showing significantly thermal stability. Fast degradation that arose around 300°C to 400°C corresponds to $\sim$ 24% weight loss due to the degradation of the polysaccharide, followed by the last mass loss and formation of carbonaceous material.

3.1.3. Vibrating Sample Magnetometer (VSM)

Figure 6 shows the magnetic hysteresis loops of $BaFe_{12}O_{19}$ nanoparticles and $BaFe_{12}O_{19}$@IM nanocomposites, which were studied using VSM analysis in the range of $-8500 < Oe < 8500$ applied field. The magnetic saturation (M_s) and coercivity (H_c) of the hard-ferromagnetic barium hexaferrite were 48.60 emu/g and 4688.98 Oe, respectively. Re-

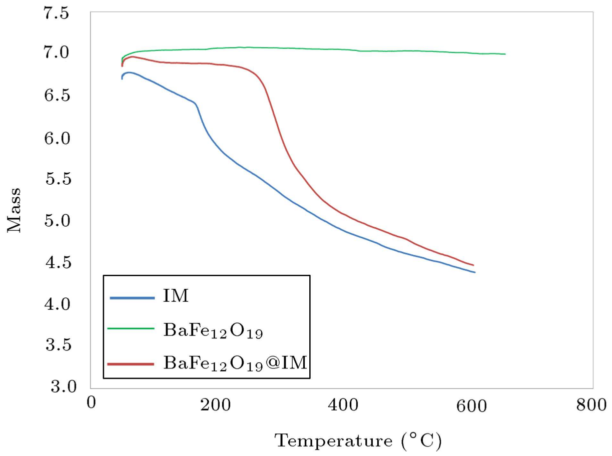

Figure 5. The thermogravimetric analysis of IM, $BaFe_2O_{19}$ and $BaFe_2O_{19}$@IM.

Table 1. Magnetic parameters of the $BaFe_{12}O_{19}$ and $BaFe_{12}O_{19}$@IM nanostructures.

Entry	**Sample**	$\boldsymbol{M_s}$ **(emu/g)**	$\boldsymbol{M_r}$ **(emu/g)**	$\boldsymbol{H_c}$ **(Oe)**
1	$BaFe_{12}O_{19}$	48.60	30.64	4688.98
2	$BaFe_{12}O_{19}$@IM	39.93	21.34	2630.93

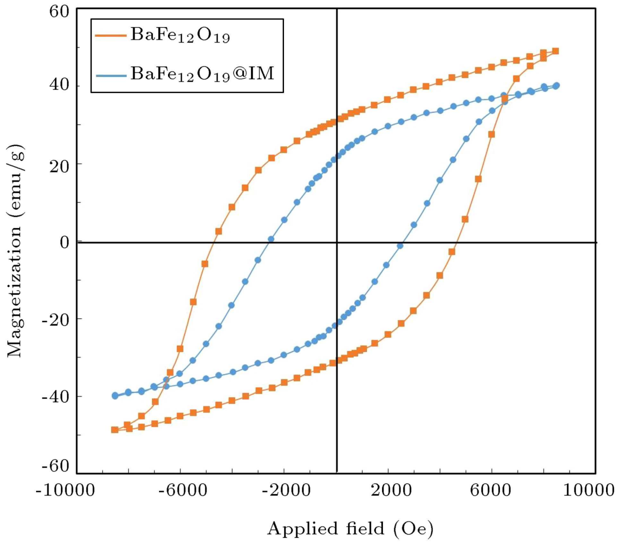

Figure 6. Magnetic hysteresis loops of the $BaFe_{12}O_{19}$ nanoparticles and $BaFe_{12}O_{19}$@IM nanocomposite.

sults indicated that the M_s of the $BaFe_{12}O_{19}$@IM nanocomposites was diminished from 48.60 emu/g to 39.93 emu/g, which was related to the mass fraction of the non-magnetic polysaccharide within the nanocomposite. $BaFe_{12}O_{19}$@IM nanocomposites also show a hard-magnetic behavior referring to their broad hysteresis loops. Magnetic reusability originated from heat resistant barium hexaferrite is the most significant feature of the $BaFe_{12}O_{19}$@IM nanocomposite. It should be noted that the magnetic property of the nanocomposite $BaFe_{12}O_{19}$@IM was good enough for easy separation in a magnetic field. Table 1 shows the magnetic parameters of $BaFe_{12}O_{19}$ nanoparticles and $BaFe_{12}O_{19}$@IM nanocomposites.

3.1.4. SEM and EDS analysis

The morphologies of IM, $BaFe_{12}O_{19}$ nanoparticles, and $BaFe_{12}O_{19}$@IM nanocomposite were investigated by SEM analysis and shown in Figure 7(a), (b) and (c), respectively. IM micrographs indicate an amorphous polymeric structure (Figure 7(a)). The SEM micrograph of the $BaFe_{12}O_1$ nanoparticles (Figure 7(b)) illustrates a uniform lace-like morphology made up of hexagonal polycrystalline nanoparticles with an average size of around 70 nm. The SEM image related to the $BaFe_{12}O_{19}$@IM nanocomposites shown in Figure 7(c) shows well that the IM surface was practically uniformly covered by hexagonal $BaFe_{12}O_{19}$ nanoparticles. The average size of $BaFe_{12}O_{19}$@IM nanocomposites is around 85 nm. The EDS analysis of $BaFe_{12}O_{19}$@IM divulges the presence of carbon, sulfur, oxygen, barium, and iron in the structure of this material (Figure 7(d)).

3.1.5. Energy dispersive X-ray (XRD)

Figure 8 shows the X-ray diffraction patterns of the bare $BaFe_{12}O_{19}$, $BaFe_{12}O_{19}$@IM, and IM. The XRD pattern of $BaFe_{12}O_{19}$ displayed distinct diffraction peaks at 2θ values = 29.92, 31.68, 33.54, 34.84, 36.54, 54.61, 56.18, and 62.84, which are related to the (110), (107), (114), (203), (217), (2011), and (220) crystal planes of $BaFe_{12}O_{19}$ based on the [01-072-0738] standard chart. The amorphous polymeric structure of the IM polysaccharide can be highlighted by a typical broad peak at 20. Also, it is clearly obvious that the crystal structure of the barium hexaferrite has been preserved after treatment by IM without any significant changes in its XRD pattern. So, the main structural peaks of the $BaFe_{12}O_{19}$@IM nanocomposite and barium hexaferrite are the same. IM peaks exhibited low intensity in the $BaFe_{12}O_{19}$@IM nanocomposite pattern relating to the robust intensity of the barium hexaferrite crystal phases, the weak peak intensity of the IM amorphous polymeric structure on the one hand and high mass fraction of the $BaFe_{12}O_{19}$ nanoparticles to the polysaccharide on the other.

3.1.6. Brunauer-Emmett-Teller (BET) analysis

The surface area, total pore volume, and average pore diameter of the $BaFe_{12}O_{19}$@IM were analyzed by N_2 adsorption-desorption analysis and found to be 17.65 m^2/g, 0.032 cm^3/g, 7.29 nm respectively. As shown in Figure 9, $BaFe_{12}O_{19}$@IM have type IV isotherms indicating mesoporous structures of the sample.

3.2. The antimicrobial activity of $BaFe_{12}O_{19}$@IM

The antibacterial activity of $BaFe_{12}O_{19}$@IM was investigated against two bacterial strains: *E. coli* and *S. aureus*. The plate of Mueller-Hinton (MH) supplemented with tween 80 surfactants (final concentration of 0.05% v/v) using an agar medium was applied. Suspensions of each bacterium were accumulated to obtain in the vicinity of 108 colony forming units (cfu) per ml for agar plating. For this purpose, 50 mg of the sample were maintained at 4°C for 2 h, and then incubated overnight at 37°C. Clear inhibition zones around the discs indicated the presence of antimicrobial

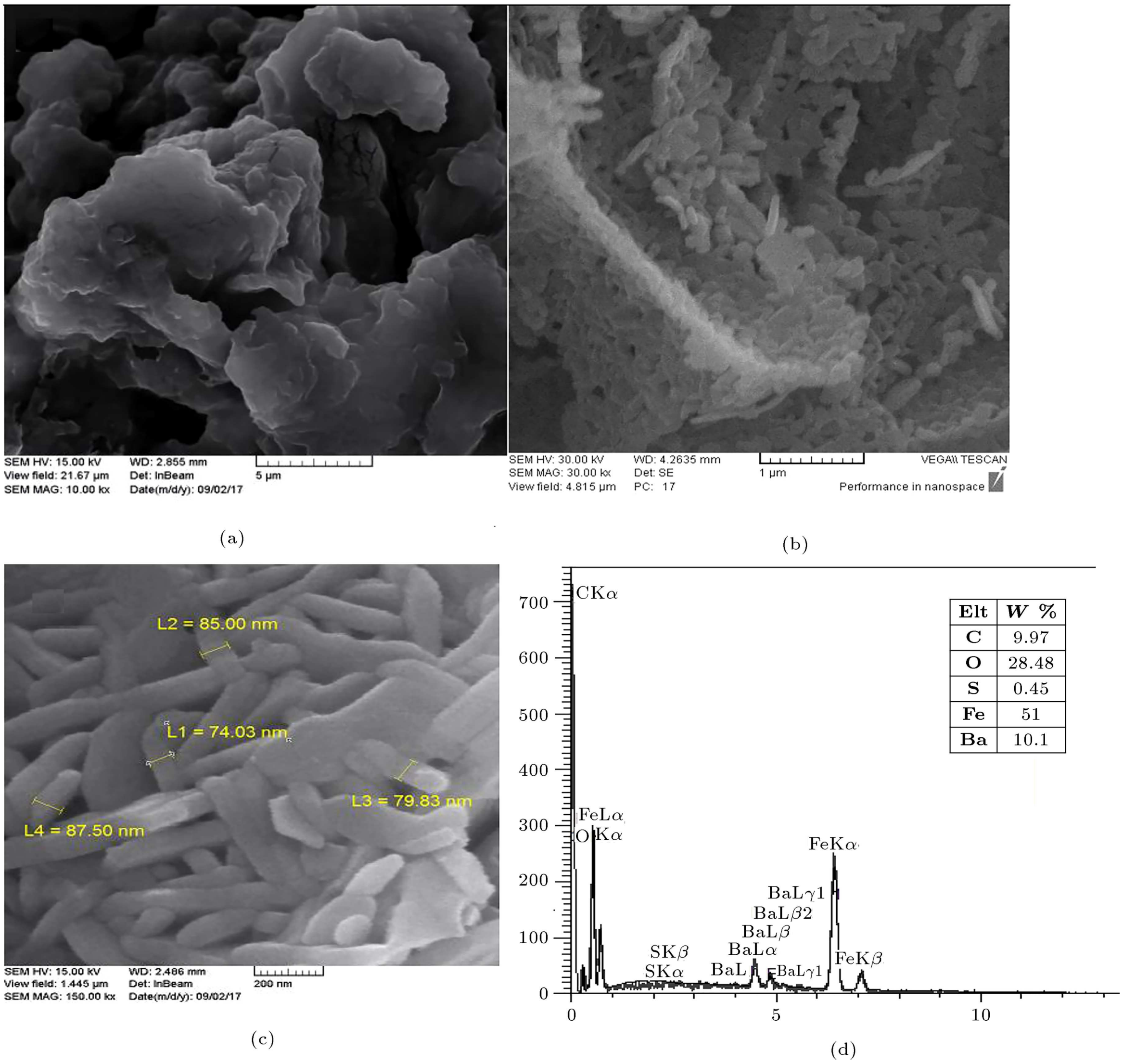

Elt	*W* %
C	9.97
O	28.48
S	0.45
Fe	51
Ba	10.1

(a) (b) (c) (d)

Figure 7. SEM images of (a) IM, (b) bare $BaFe_{12}O_{19}$ nanoparticles, (c) $BaFe_{12}O_{19}$@IM nanocomposite, and (d) EDS analysis of $BaFe_{12}O_{19}$@IM nanocomposite.

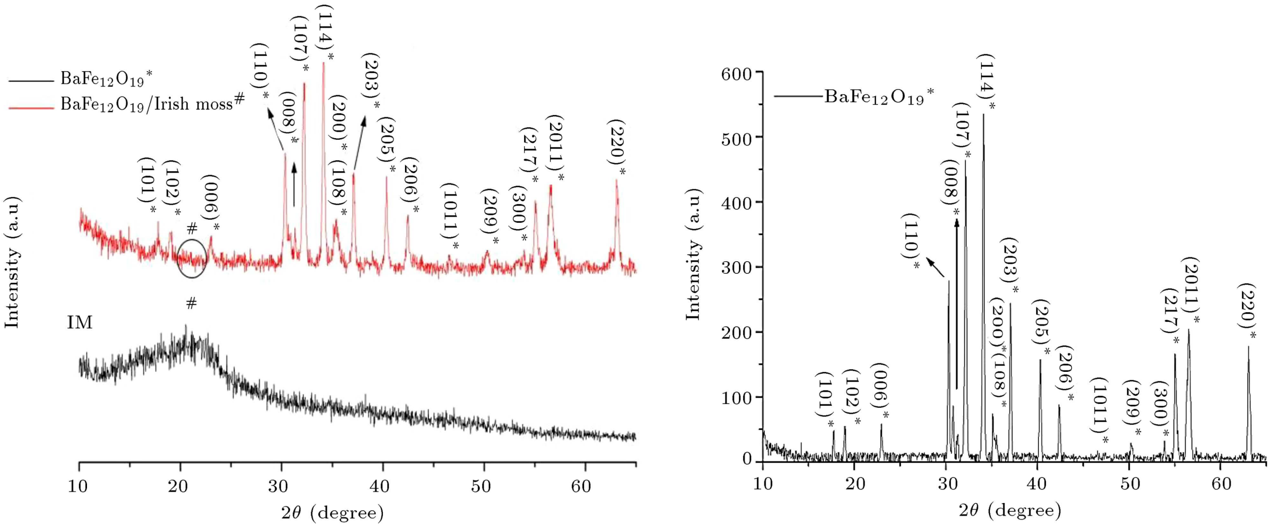

Figure 8. X-ray diffraction patterns of the bare $BaFe_{12}O_{19}$, IM, and $BaFe_{12}O_{19}$@IM.

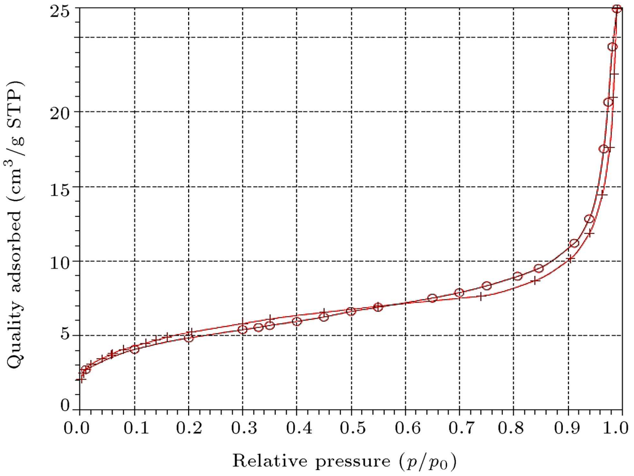

Figure 9. BET curve of $BaFe_{12}O_{19}$@IM.

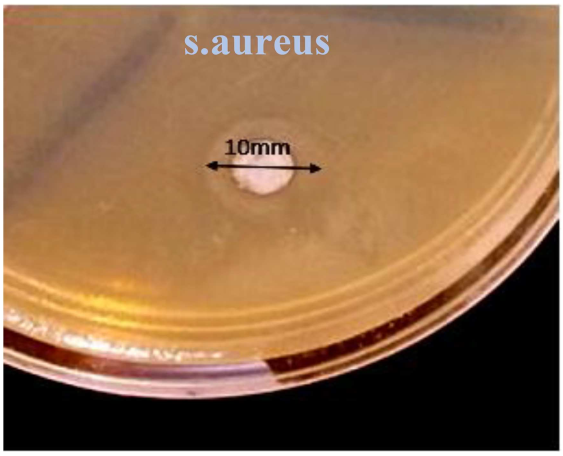

Figure 10. Antibacterial activity of $BaFe_{12}O_{19}$@IM against *S. aureus*.

activity. The diameter of the clear inhibition zone around the $BaFe_{12}O_{19}$@IM disc is 10 mm for *S. aureus*, whereas no obvious growth was detected for *E. coli.* (Figure 10).

3.3. Catalytic activity of $BaFe_{12}O_{19}$@IM

The catalytic activity of the heterogeneous $BaFe_{12}O_{19}$@IM nanocomposite for the preparation of benzopyranopyrimidines was investigated. For this purpose, the pseudo four-component condensation reaction of salicylaldehyde, malononitrile and morpholine as a model reaction was studied. Some relevant results of these reactions are summarized in Table 2. In the beginning, the reaction was undertaken under catalyst-free conditions and there was not any progress in this situation (Table 2, entry 13). In the presence of $BaFe_{12}O_{19}$ MNPs and IM, the reaction proceeded with 30% and 60% yields, respectively (Table 2, entries 5, 6). However, the modified catalyst $BaFe_{12}O_{19}$@IM nanocomposite increased the yield of reaction up to 95% (Table 2, entry 2) due to the synergistic effects of $BaFe_{12}O_{19}$ and IM. To determine the efficiency of the catalyst concentration, some experiments were probed in the presence of different amounts of the catalyst (5, 10, 15, 20 mg), giving benzopyranopyrimidines with 80%, 90%, 95% and 95% isolated yields. Thus, the best yield is accessible in the presence of just a 15 mg catalyst, and using more amounts of the catalyst did not increase the result to a considerable level (Table 2, entries 1–4). The optimal amount of $BaFe_{12}O_{19}$ @IM catalyst (15 mg) has been examined in various solvents. Under solvent-free conditions, a trace of the product was produced (Table 2, entry 12). Satisfactory results have been obtained with polar protic solvents such as H_2O, MeOH, and EtOH (Table 2, entries 2, 7, 8), rather than nonpolar or polar aprotic solvents such as CH_2Cl_2, Toluene, CH_3CN (Table 2, entries 9, 10, 11).

Table 2. Optimization of the $BaFe_{12}O_{19}$@IM nanocomposite for synthesis of the benzopyranopyrimidine derivatives (**3j**)^a.

Entry	Catalyst (mg)	Solvent	Yield (%)^b
1	$BaFe_{12}O_{19}$@IM (20 mg)	EtOH	95
2	$BaFe_{12}O_{19}$@IM (15 mg)	EtOH	95
3	$BaFe_{12}O_{19}$@IM (10 mg)	EtOH	90
4	$BaFe_{12}O_{19}$@IM (5 mg)	EtOH	80
5	$BaFe_{12}O_{19}$ (15 mol%)	EtOH	30
6	IM (15 mg)	EtOH	60
7	$BaFe_{12}O_{19}$@IM (15 mg)	H_2O	70
8	$BaFe_{12}O_{19}$@IM (15 mg)	MeOH	75
9	$BaFe_{12}O_{19}$@IM (15 mg)	CH_2Cl_2	35
10	$BaFe_{12}O_{19}$@IM (15 mg)	Toluene	40
11	$BaFe_{12}O_{19}$@IM (15 mg)	CH_3CN	75
12	$BaFe_{12}O_{19}$@IM (15 mg)	—	25
13	No catalyst	EtOH	Nil

^{a}: Reaction conditions: salicylaldehyde (2 mmol), morpholine (1 mmol), malononitrile (1 mmol), catalyst, solvent (4 mL), room temperature.

^{b}: Isolated yields.

Various derivatives of salicylaldehyde and secondary amines were perused under optimized reaction conditions, and the results are shown in (Table 3). The vast range of salicylaldehyde substitution can produce a reaction from electron-withdrawing groups like halogens up to electron-donating substituents such as the methoxy group. All products are known compounds, almost all the reactions worked quite well, and the desired products were obtained in good to high yields.

A comparison between the presented protocol in this study and other reported protocols for the same model reaction has been reported in Table 4. According to these results, the yield of benzopyranopyrimidine

Table 3. The pseudo four-component preparation of benzopyranopyrimidines catalyzed by $BaFe_{12}O_{19}$@IM nanocomposite[a].

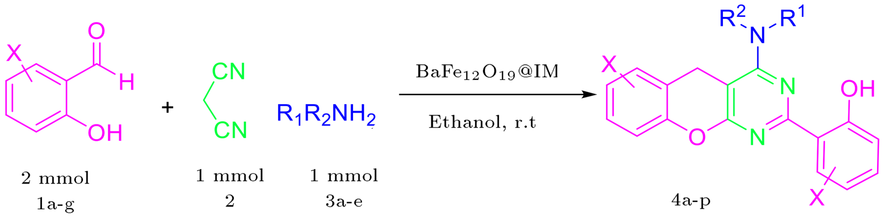

Entry	Aldehyde	Amine	Product	Yields[b] (%)	M.p. (°C) Found/Ref.
1	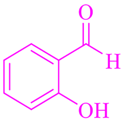	Morpholine	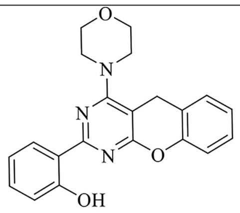 **4a**	95	197-199/196-197 [40]
2	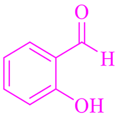	Piperidine	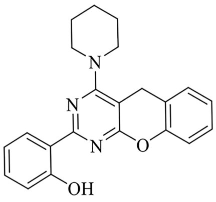 **4b**	95	167-179/168-170 [32]
3	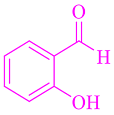	Dimethylamine	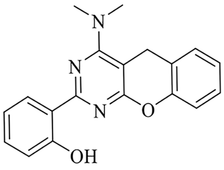 **4c**	90	180-183/177-179 [32]
4	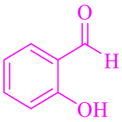	Pyrrolidine	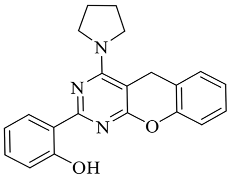 **4d**	80	235-237/235-237 [34]
5	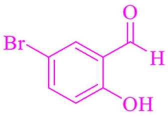	Morpholine	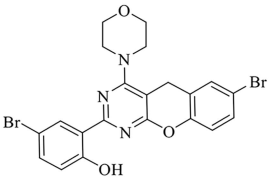 **4f**	83	200/194-196 [43]
6	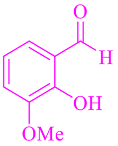	Morpholine	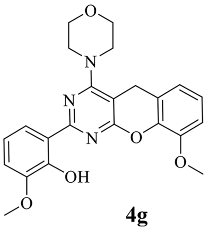 **4g**	85	212-215/210-220 [44]

[a]: Reaction conditions: Salicylaldehyde derivatives (2 mmol), amines (1 mmol), malononitrile (1 mmol), $BaFe_{12}O_{19}$@IM (0.015 g), solvent (4 mL), room temperature;

[b]: Isolated yields.

Table 3. The pseudo four-component preparation of benzopyranopyrimidines catalyzed by BaFe$_{12}$O$_{19}$@IM nanocomposite[a] (continued).

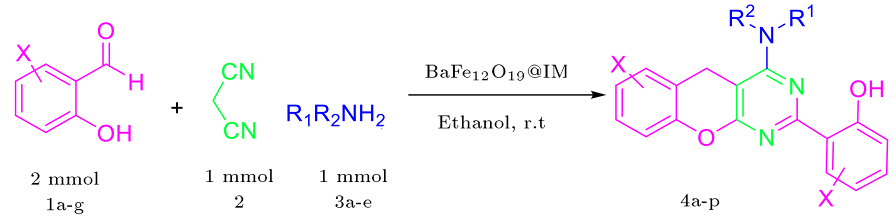

Entry	Aldehyde	Amine	Product	Yields[b] (%)	M.p. (°C) Found/Ref.
7	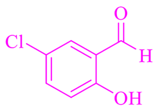	Morpholine	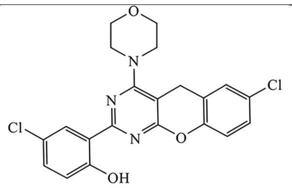 **4h**	90	249-251/247-250 [45]
8	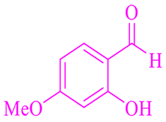	Diethylamine	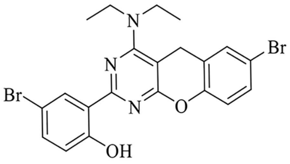 **4i**	75	175-178/178-179 [46]
9	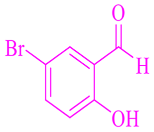	Piperidine	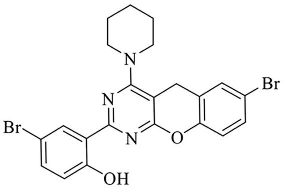 **4j**	80	222-225/226 [43]
10	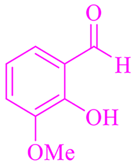	Piperidine	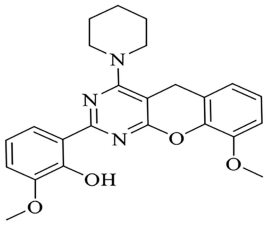 **4k**	92	176-179/178-180 [44]
11	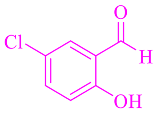	pyrolidine	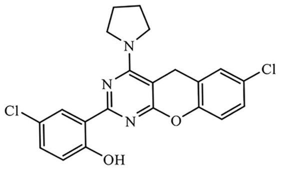 **4l**	96	192-194/191-194 [47]
12	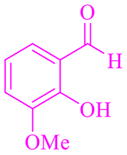	pyrolidine	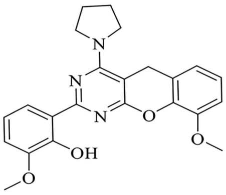 **4m**	95	157-159/158-160 [43]

[a]: Reaction conditions: Salicylaldehyde derivatives (2 mmol), amines (1 mmol), malononitrile (1 mmol), BaFe$_{12}$O$_{19}$@IM (0.015 g), solvent (4 mL), room temperature;

[b]: Isolated yields.

Table 3. The pseudo four-component preparation of benzopyranopyrimidines catalyzed by $BaFe_{12}O_{19}$@IM nanocomposite[a] (continued).

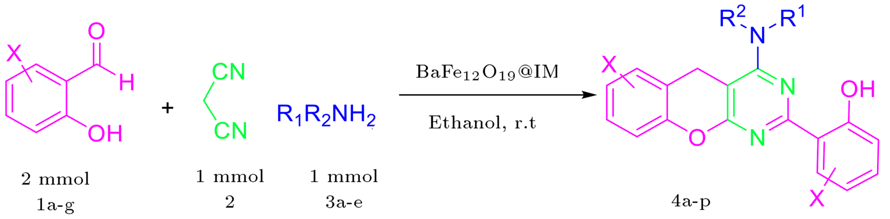

Entry	Aldehyde	Amine	Product	Yields[b] (%)	M.p. (°C) Found/Ref.
13	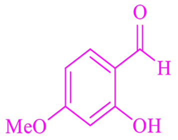	Dimethylamine	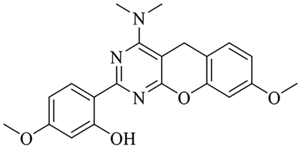 **4n**	93	179-181/180-182 [48]
14	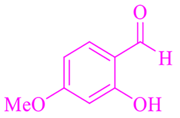	Morpholine	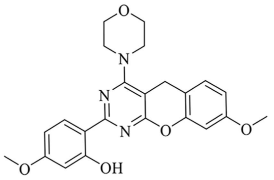 **4o**	89	210-213/210-212 [49]
15	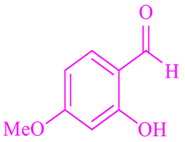	pyrolidine	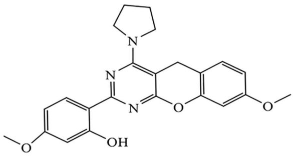 **4p**	91	158-162/159-161 [47]

[a]: Reaction conditions: Salicylaldehyde derivatives (2 mmol), amines (1 mmol), malononitrile (1 mmol), $BaFe_{12}O_{19}$@IM (0.015 g), solvent (4 mL), room temperature;

[b]: Isolated yields.

Table 4. Comparison of the activity of the catalysts for the synthesis of benzopyranopyrimidine (**4a**) with some of the other catalysts reported in the literature.

Entry	Catalyst	Reaction condition	Reaction time (h)	Yield (%)	Reference
1	$LiClO_4$	Ethanol, rt	24	84	[32]
2	Piperidine	100°C	11	78	[33]
3	Fe(II)-BTU-SNPs	Ethanol, rt	4	93	[34]
4	Tetrabromobenzene-1,3-disulfonamide	Ethanol, rt	24	90	[42]
5	Fe_3O_4/IRMOF-3/SO_3H	Ethanol, rt	1	95	[36]
6	*p*-toluenesulfonic acid	Solvent-free, rt	1	75	[50]
7	$BaFe_{12}O_{19}$@IM	Ethanol, rt	1	95	This work

production in the present study was 95%, which is effectively better than the other projects with different catalysts. Also, in terms of reaction time, the production of benzopyranopyrimidine was 1 hour which is lower than the other projects. Totally, these two differences between present and prior results can confirm the efficiency of this project.

The proposed mechanism for the formation of the benzopyranopyrimidines with the desired consequence of the catalytic activity of $BaFe_{12}O_{19}$@IM nano-catalyst is shown in Figure 11. Referring to the suggested mechanism, Brønsted acidic sites of the catalyst, i.e. -OH and metal positively-charged metal ions (Fe^{3+}, Ba^{2+}), which facilitate the Knoevenagel

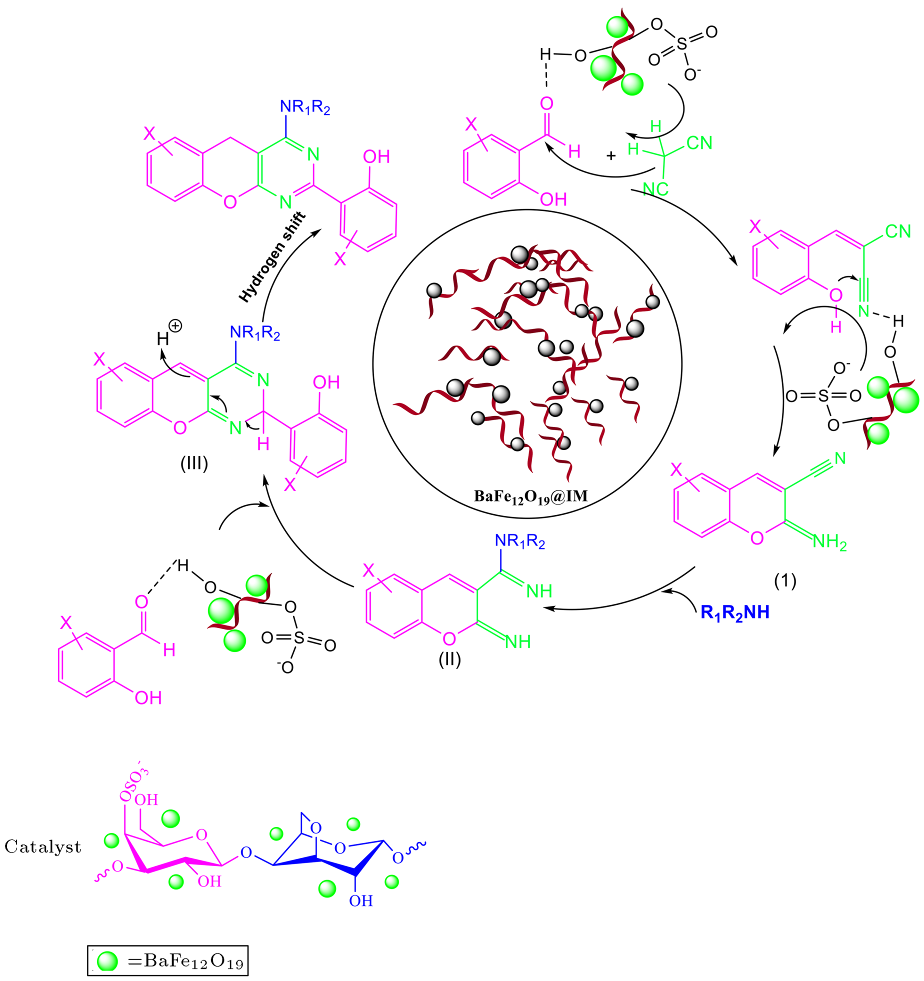

Figure 11. Proposed mechanism for the synthesis of benzopyranopyrimidines in the presence of $BaFe_{12}O_{19}$@IM magnetic nanocomposites.

condensation reaction, might activate the carbonyl group of salicylic aldehyde toward nucleophilic attack of the malononitrile anion generated by Lewis basic sites of IM ($-OSO_3^-$) and (O^{2-}) of $BaFe_{12}O_{19}$ in the catalyst. On the other hand, these Lewis basic sites in the catalyst, by activating the phenolic O-H groups, trigger the Pinner reaction which leads to the intermediate (I). Following that, the intermediate (II) is produced by the attack of the amine on the cyano group. Ultimately, intermediate (II) reacts with another salicylic aldehyde, giving rise to the intermediate (III), followed by hydrogen transfer to yield the final benzopyranopyrimidine. In fact, the formation of the product results from the activation of the reactants by the brønsted basic and acidic catalyst sites.

4. Conclusions

In conclusion, a natural polymer supported biomagnetic material, $BaFe_{12}O_{19}$@IM, has been prepared using a simple sol-gel method. The catalytic activity of this biomagnetic material, as a heterogeneous bifunctional acid-base catalyst, has been investigated in the synthesis of benzopyranopyrimidine derivatives. As the results have shown, the separation of this biomagnetic catalyst is very easy thanks to the effective magnetic property of $BaFe_{12}O_{19}$. The bifunctional character of the catalyst due to the existence of sulfate and hydroxyl groups in sulfated polysaccharide, together with the greater surface accessibility of these functional groups, besides the magnetic characteristic of the catalyst, are the key factors for catalytic performance, easy separation, and recyclability of $BaFe_{12}O_{19}$@IM. Study on the antibacterial performance of $BaFe_{12}O_{19}$@IM nanocomposites on bacteria strains was evaluated. The results showed that the prepared nanocomposites possess antibacterial activity against Gram-positive *S. aureus*.

Acknowledgement

The authors gratefully acknowledge the support of the Research Council of Iran University of Science and Technology, Tehran, Iran.

References

1. Wu, W., He, Q., and Jiang, C. "Magnetic iron oxide nanoparticles: synthesis and surface functionalization strategies", *Nanoscale Res. Lett.*, **3**(11), p. 397 (2008).
2. Stanciu, L., Won, Y.H., Ganesana, M., et al. "Magnetic particle-based hybrid platforms for bioanalytical sensors", *Sensors*, **9**(4), pp. 2976–2999 (2009).
3. Hudson, R., Feng, Y., Varma, R.S., et al. "Bare magnetic nanoparticles: sustainable synthesis and applications in catalytic organic transformations", *Green Chemistry*, **16**(10), pp. 4493–4505 (2014).
4. Kheilkordi, Z., Ziarani, G.M., Lashgari, N., et al. "An efficient method for the synthesis of functionalized 4H-chromenes as optical sensor for detection of Fe3+ in ethanol", *Polyhedron*, **166**, pp. 203–209 (2019).
5. Hessien, M.M. and Khedr, M.H. "Catalytic activity and magnetic properties of barium hexaferrite prepared from barite ore", *Mater. Res. Bull.*, **42**(7), pp. 1242–1250 (2007).
6. Liu, X., Zhang, T., Xu, D., et al. "Microwave-assisted catalytic degradation of crystal violet with barium ferrite nanomaterial", *Ind. Eng. Chem. Res.*, **55**(46), pp. 11869–11877 (2016).
7. Haijun, Z., Zhichao, L., Chengliang, M., et al. "Complex permittivity, permeability, and microwave absorption of Zn-and Ti-substituted barium ferrite by citrate sol-gel process", *Mater. Sci. Eng., B.*, **96**(3), pp. 289–295 (2002).
8. Palla, B.J., Shah, D.O., Garcia-Casillas, P., et al. "Preparation of nanoparticles of barium ferrite from precipitation in microemulsions", *J. Nanopart. Res.*, **1**(2), pp. 215–221 (1999).
9. Piri, T., Peymanfar, R., Javanshir, S., et al. "Magnetic $BaFe_{12}O_{19}/Al_2O_3$: An efficient heterogeneous Lewis acid catalyst for the synthesis of α-aminophosphonates (Kabachnik-fields reaction)", *Catal. Lett.*, **149**(12), pp. 3384–3394 (2019).
10. Peymanfar, R., Ahmadi, M., and Javanshir, S. "Tailoring GO/$BaFe_{12}O_{19}$/La0.5Sr0.5MnO_3 ternary nanocomposite and investigation of its microwave characteristics", *Mater. Res. Express*, **6**(8), p. 085063 (2019).
11. Zheng, Y., Monty, J., and Linhardt, R.J. "Polysaccharide-based nanocomposites and their applications", *Carbohydr. Res.*, **405**, pp. 23–32 (2015).
12. Pourjavadi, A., Hosseini, S.H., Seidi, F., et al. "Magnetic removal of crystal violet from aqueous solutions using polysaccharide-based magnetic nanocomposite hydrogels", *Polym. Int.*, **62**(7), pp. 1038–1044 (2013).
13. Mahdavinasab, M., Hamzehloueian, M., and Sarrafi, Y. "Preparation and application of magnetic chitosan/graphene oxide composite supported copper as a recyclable heterogeneous nanocatalyst in the synthesis of triazoles", *Int. J. Biol. Macromol.*, **138**, pp. 764–772 (2019).
14. Grüttner, C., Rudershausen, S., and Teller, J. "Improved properties of magnetic particles by combination of different polymer materials as particle matrix", *J. Magn. Magn. Mater.*, **225**(1–2), pp. 1–7 (2001).
15. Maleki, A., Varzi, Z., and Hassanzadeh-Afruzi, F. "Preparation and characterization of an eco-friendly ZnFe2O_4@ alginic acid nanocomposite catalyst and its application in the synthesis of 2-amino-3-cyano-4H-pyran derivatives", *Polyhedron*, **171**, pp. 193–202 (2019).
16. Chang, P.R., Yu, J., Ma, X., et al. "Polysaccharides as stabilizers for the synthesis of magnetic nanoparticles", *Carbohydr. Polym.*, **83**(2), pp. 640–644 (2011).
17. Salehi, M.H., Yousefi, M., Hekmati, M., et al. "In situ biosynthesis of palladium nanoparticles on Artemisia abrotanum extract-modified graphene oxide and its catalytic activity for Suzuki coupling reactions", *Polyhedron*, **165**, pp. 132–137 (2019).
18. Dolatkhah, Z., Javanshir, S., Bazgir, A., et al. "Palladium on magnetic Irish moss: A new nano-biocatalyst for suzuki type cross-coupling reactions", *Appl. Organomet. Chem.*, **33**(7), p. e4859 (2019).
19. Hemmati, B., Javanshir, S., and Dolatkhah, Z. "Hybrid magnetic Irish moss/Fe_3O_4 as a nano-biocatalyst for synthesis of imidazopyrimidine derivatives", *RSC Adv.*, **6**(56), pp. 50431–50436 (2016).
20. Rudtanatip, T., Lynch, S.A., Wongprasert, K., et al. "Assessment of the effects of sulfated polysaccharides extracted from the red seaweed Irish moss Chondrus crispus on the immune-stimulant activity in mussels Mytilus spp", *Fish Shellfish Immunol.*, **75**, pp. 284–290 (2018).
21. Lee, J., Ghosh, S., and Saier Jr, M.H. "Comparative genomic analyses of transport proteins encoded within the red algae Chondrus crispus, Galdieria sulphuraria, and Cyanidioschyzon merolae11",*J. Phycol.*, **53**(3), pp. 503–521 (2017).
22. Prajapati, V.D., Maheriya, P.M., Jani, G.K., et al. "RETRACTED: Carrageenan: A natural seaweed polysaccharide and its applications", *Carbohydr. Polym.*, **105**, pp. 97–112 (2014).
23. Gordon Young, E. and Goring, D.A.I. "The stability of carrageenin in dried Irish moss (Chondrus crispus)", *J. Sci. Food Agric.*, **9**(9), pp. 539–541 (1958).
24. Zaheri, H.M., Javanshir, S., Hemmati, B., et al. "Magnetic core-shell Carrageenan moss/Fe_3O_4: a polysaccharide-based metallic nanoparticle for synthesis of pyrimidinone derivatives via Biginelli reaction", *Chem. Cent. J.*, **12**(1), p. 108 (2018).
25. Safari, J. and Javadian, L. "Ultrasound assisted the green synthesis of 2-amino-4H-chromene derivatives catalyzed by Fe_3O_4-functionalized nanoparticles with chitosan as a novel and reusable magnetic catalyst", *Ultrason. Sonochem.*, **22**, pp. 341–348 (2015).
26. Murugadoss, A. and Chattopadhyay, A. "A 'green' chitosan-silver nanoparticle composite as a heterogeneous as well as micro-heterogeneous catalyst", *Nanotechnology*, **19**(1), p. 015603 (2007).

27. Movassagh, B. and Rezaei, N. "A magnetic porous chitosan-based palladium catalyst: a green, highly efficient and reusable catalyst for Mizoroki-Heck reaction in aqueous media", *New J. Chem.*, **39**(10), pp. 7988–7997 (2015).

28. Saikia, G., Ahmed, K., Gogoi, S.R., et al. "A chitosan supported peroxidovanadium (V) complex: Synthesis, characterization and application as an eco-compatible heterogeneous catalyst for selective sulfoxidation in water", *Polyhedron*, **159**, pp. 192–205 (2019).

29. Wu, W.B., Chen, S.H., Hou, J.Q., et al. "Disubstituted 2-phenyl-benzopyranopyrimidine derivatives as a new type of highly selective ligands for telomeric G-quadruplex DNA", *Org. Biomol. Chem.*, **9**(8), pp. 2975–2986 (2011).

30. Bruno, O., Brullo, C., Schenone, S., et al. "Synthesis, antiplatelet and antithrombotic activities of new 2-substituted benzopyrano [4, 3-d] pyrimidin-4-cycloamines and 4-amino/cycloamino-benzopyrano [4, 3-d] pyrimidin-5-ones", *Bioorg. Med. Chem.*, **14**(1), pp. 121–130 (2006).

31. Bajda, M., Guzior, N., Ignasik, M., et al. "Multi-target-directed ligands in Alzheimer's disease treatment", *Curr. Med. Chem.*, **18**(32), pp. 4949–4975 (2011).

32. Ghahremanzadeh, R., Amanpour, T., and Bazgir, A. "Pseudo four-component synthesis of benzopyranopyrimidines", *Tetrahedron Lett.*, **51**(32), pp. 4202–4204 (2010).

33. Zonouzi, A., Biniaz, M., and Mirzazadeh, R. "An efficient one-pot and solvent-free synthesis of chromeno [2, 3-d] pyrimidine derivatives: microwave assisted reaction", *Heterocycles*, **81**(5), pp. 1271–1278 (2010).

34. Amirnejat, S., Movahedi, F., Masrouri, H., et al. "Silica nanoparticles immobilized benzoylthiourea ferrous complex as an efficient and reusable catalyst for one-pot synthesis of benzopyranopyrimidines", *J. Mol. Catal. A: Chem.*, **378**, pp. 135–141 (2013).

35. Niknam, K. and Borazjani, N. "Synthesis of benzopyrano [2, 3-d] pyrimidines using silica-bonded N-propyldiethylenetriamine sulfamic acid (SPDTSA) as heterogeneous solid acid catalyst under solvent-free conditions", *Org. Chem. Res.*, **1**(1), pp. 78–86 (2015).

36. Mostafavi, M.M. and Movahedi, F. "Synthesis, characterization, and heterogeneous catalytic activity of sulfamic acid functionalized magnetic IRMOF-3", *Eur. J. Org. Chem.*, **2019**(6), pp. 787–793 (2019).

37. Kanakaraju, S., Prasanna, B., Basavoju, S., et al. "Ionic liquid catalyzed one-pot multi-component synthesis, characterization and antibacterial activity of novel chromeno [2, 3-d] pyrimidin-8-amine derivatives", *J. Mol. Struct.*, **1017**, pp. 60–64 (2012).

38. Ballabeni, V., Calcina, F., Tognolini, M., et al. "Effects of subacute treatment with benzopyranopyrimidines in hemostasis and experimental thrombosis in mice", *Life Sci.*, **74**(15), pp. 1851–1859 (2004).

39. Bruno, O., Brullo, C., Bondavalli, F., et al. "2-Amino/azido/hydrazino-5-alkoxy-5H-[1] benzopyrano [4, 3-d] pyrimidines: synthesis and pharmacological evaluation", *Med. Chem.*, **3**(2), pp. 127–134 (2007).

40. Gupta, A.K., Kumari, K., Singh, N., et al. "An eco-safe approach to benzopyranopyrimidines and 4H-chromenes in ionic liquid at room temperature", *Tetrahedron Lett.*, **53**(6), pp. 650–653 (2012).

41. Shaterian, H.R. and Aghakhanizadeh, M. "Mild preparation of chromeno [2, 3-d] pyrimidines catalyzed by Brønsted acidic ionic liquids under solvent-free and ambient conditions", *Res. Chem. Intermed.*, **39**(8), pp. 3877–3885 (2013).

42. Ghorbani-Vaghei, R., Shirzadi-Ahodashti, M., Eslami, F., et al. "Efficient one-pot synthesis of quinazoline and benzopyrano [2, 3-d] pyrimidine derivatives catalyzed by N-bromosulfonamides", *J. Heterocycl. Chem.*, **54**(1), pp. 215–225 (2017).

43. Umamahesh, B., Mandlimath, T.R., and Sathiyanarayanan, K.I. "A novel, facile, rapid, solvent free protocol for the one pot green synthesis of chromeno [2, 3-d] pyrimidines using reusable nano $ZnAl_2O_4$-a NOSE approach and photophysical studies", *RSC Adv.*, **5**(9), pp. 6578–6587 (2014).

44. Kabeer, S.A., Reddy, G.R., Sreelakshmi, P., et al. "TiO_2-SiO_2 catalyzed eco-friendly synthesis and antioxidant activity of benzopyrano [2, 3-d] pyrimidine derivatives", *J. Heterocycl. Chem.*, **54**(5), pp. 2598–2604 (2017).

45. Thirupathaiah, B., Reddy, M.V., and Jeong, Y.T. "Solvent-free sonochemical multi-component synthesis of benzopyranopyrimidines catalyzed by polystyrene supported p-toluenesulfonic acid", *Tetrahedron*, **71**(14), pp. 2168–2176 (2015).

46. Zonouzi, A., Hosseinzadeh, F., Karimi, N., et al. "Novel approaches for the synthesis of a library of fluorescent chromenopyrimidine derivatives", *ACS Comb. Sci.*, **15**(5), pp. 240–246 (2013).

47. Nasab, M.J. and Kiasat, A.R. "Covalently anchored 2-amino ethyl-3-propyl imidazolium bromideon SBA-15 as a green, efficient and reusable Brønsted basic ionic liquid nanocatalyst for one-pot solvent-free synthesis of benzopyranopyrimidines under ultrasonic irradiation", *RSC Adv.*, **5**(92), pp. 75491–75499 (2015).

48. Niknam, K. and Borazjani, N. "Synthesis of benzopyrano [2, 3-d] pyrimidines using silica-bonded N-propylpiperazine sodium N-propionate as heterogeneous solid base catalyst under solvent-free conditions", *Monatsh. Chem.*, **147**(6), pp. 1129–1135 (2016).

49. Kour, G. and Gupta, M. "A nano silver-xerogel (Ag nps@ modified TEOS) as a newly developed nanocatalyst in the synthesis of benzopyranopyrimidines (with secondary and primary amines) and gem-bisamides", *Dalton Trans.*, **46**(21), pp. 7039–7050 (2017).

50. Thirupathaiah, B., Reddy, M.V., and Jeong, Y.T. "Solvent-free sonochemical multi-component synthesis of benzopyranopyrimidines catalyzed by polystyrene supported p-toluenesulfonic acid", *Tetrahedron*, **71**(14), pp. 2168–2176 (2015).

Biographies

Sara Amirnejat obtained her BS degree in Chemistry from Alzahra University, Iran in 2009, her MS degree in Organic Chemistry from the University of Tarbiyat Modares, Tehran, Iran in 2012, and her PhD degree in Organic Chemistry, in 2020, from Iran University of Science and Technology, Tehran, Iran.

Shahrzad Javanshir received her BS and MS degrees in Chemistry and Organic Chemistry in 1983 and 1985, respectively, from the University of Claude Bernard Lyon I, France, and her PhD degree in Organic Chemistry, in 2007, from Alzahra University, Tehran, Iran. She is currently Assistant Professor of Organic Chemistry at Iran University of Science and Technology. Tehran, Iran. Her research interests include organic synthesis (heterocyclic and medicinal chemistry), green chemistry and catalysis.